JACS
JOURNAL OF THE AMERICAN CHEMICAL SOCIETY
ARTICLE
pubs.acs.org/JACS

Finite Size Effect of Proton-Conductivity of Amorphous Silicate Thin Films Based on Mesoscopic Fluctuation of Glass Network

Yoshitaka Aoki,[*,†] Hiroki Habazaki,[†] Shinji Nagata,[‡] Aiko Nakao,[⊥] Toyoki Kunitake,[⊥] and Shu Yamaguchi[#]

[†]Faculty of Engineering, Hokkaido University, N13W8, Kita-ku, Sapporo, 060-8628, Japan
[‡]Institute for Materials Research, Tohoku University, 2-1-1 Katahira, Sendai 980-8577, Japan
[⊥]Institute for Physical and Chemical Research (RIKEN), Hirosawa 2-1, Wako, 351-0012, Japan
[#]Department of Materials Science, The University of Tokyo, 7-3-1 Hongo, Bunkyo-ku, Tokyo 113-8656, Japan

ABSTRACT: The finite size effect of proton conductivity of amorphous silicate thin films, a-$M_{0.1}Si_{0.9}O_x$ (M = Al, Ga, Hf, Ti, Ta, and La), was investigated. The proton conductivity across films, σ, was measured in dry air by changing the thickness in the range of 10−1000 nm. σ of the films with M = Al, Ga, and Ta was elevated in a power law by decreasing thickness into less than a few hundred nanometers, and the increment was saturated at a thickness of several 10's of nanometers. On the other hand, σ of the films with M = Hf, Ti, and La was not related to the decrease of the thickness in the range of >10 nm. Thickness-dependent conductivity of the former could be numerically simulated by a percolative resistor network model that involves the randomly distributed array of two kinds of resistors R_1 and R_2 ($R_1 > R_2$) in the form of a simple cubic-type lattice. High-resolution TEM clarified that a-$M_{0.1}Si_{0.9}O_x$ films involved heterogeneous microstructures made of the condensed domain and the surrounding uncondensed matrix due to the fluctuation of glass networks on the nanometer scale. The condensed domain had a wormlike shape with an average length of several 10's of nanometers and performed the role of the proton conduction pathway penetrating through the poorly conducting matrix. It was concluded that the thickness-dependent conductivity could be identical to finite-size scaling of the percolative network of the interconnected domains in the nanometer range.

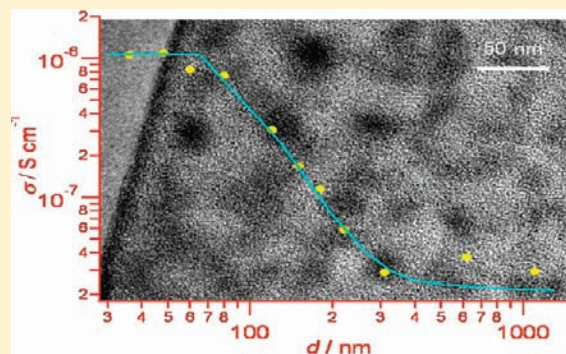

INTRODUCTION

The development of artificial solid electrolytes that possess high ionic conductivity at relatively low temperatures is of great challenge for materials chemists, since it is essential to increase efficiency and lifetime of the solid-state electrochemical devices such as a solid-state fuel cell,[1,2] all-solid-state battery,[3,4] membrane reactor,[5] memristic switch,[6,7] and so on. Recently, more and more evidence of the importance of nanoscale structure in relation to ionic conductivity has been compiled,[8−18] not only where strong variations in the conductivities are achieved but also where qualitative effects such as changing the type of conductivity could be observed. In more recent years, it was reported that the conductivity of some ionic glass films is dramatically enhanced by reducing thickness into the mesoscopic region.[15−18] The relatively high ion-conducting pathways can be locally formed inside a glass matrix because its heterogeneous structure provides distributed potential for ionic diffusion in various lengths.[19] When the thickness of glass bulk decreases to the range of the mean length of the ion-conducting pathways, the pathway percolating from edge to edge is formed, and thus the overall conductivity across film must be increased. However, the full mechanism, especially that of microstructures taking on the role of ionic channels in glass networks, is still unclear.[18−20] Hence, it is a motivation to investigate the mesoscopic situation of ionic conductivity of glassy thin films.

Since the pioneer work by Hibino et al.,[21] silicate compounds such as zeolites attract much attention as solid electrolytes which possess efficient proton conductivity at elevated temperatures even in a nonhumidified atmosphere due to the presence of the acidic protons of the Brønsted site on the anionic silicate framework.[21,22] Such a material is very promising for the next-generation intermediate temperature solid-state fuel cell (IT-FC) that operates in a temperature range of 150−400 °C.[23−25] Previously, we reported that the aluminosilicate $Al_{0.1}Si_{0.9}O_x$ thin film showed increase of proton conductivity along the thickness direction in a power law by decreasing thickness to less than 100 nm.[18] This feature might be essential for a group of amorphous silicate compounds. In fact, the various amorphous silicate thin films, a-$M_{0.1}Si_{0.9}O_x$ (M = Al, Zr, Hf, etc.), exhibit the efficient proton conductivity in nonfumidified, dry atmosphere owing to the Brønsted acidity.[26,27] Therefore, it is of fundamental and technological interest to study the thickness dependency of proton conductivity of these films. Herein, we report on the

Received: October 13, 2010
Published: February 17, 2011

ACS Publications © 2011 American Chemical Society

thickness dependency of the proton conductivity in amorphous films of various metal silicates, a-$M_{0.1}Si_{0.9}O_x$ (M = Al, Hf, Ta, Ga, La, and Ti), in the nanoscale thickness region. Some of the silicates show the remarkable enhancement of the conductivity along the thickness direction by reducing the thickness to less than a few hundred nanometers. It is demonstrated that this finite-size effect originates from the percolation of the ion-conductive domains which are formed inside the film by the nanoscale fluctuation in density and composition of the glass network. The current results could be extended to a more general way to design the ionic transport properties of various non-equilibrium materials.

EXPERIMENTAL SECTION

Thin films of various metal silicates, $M_{0.1}Si_{0.9}O_x$ (M = Al, Ti, Hf, La, Ta, and Ga), were prepared from mixed precursor solutions of tetraethoxysilane (TEOS) and individual metal alkoxides ($M(OR)_n$) with the fixed M/Si atomic ratio of 5/95, as reported elsewhere.[26,27] TEOS (99.99%) and titanium tetra-n-butoxide ($Ti(O^nBu)_4$, 98%) and tantalum penta-n-butoxide ($Ta(O^nBu)_4$, 99.9%) were obtained from Kanto Chemical. Lanthanum trimethoxyethoxide ($La(OEtOMe)_3$, 10 wt % in 1-methoxyethanol) and gallium triethoxide ($Ga(OEt)_3$, 99%) were obtained from Gelest. The films were deposited on an electrode substrate in the layer-by-layer fashion by multiple spin-coating and hydrolysis. The precursor sol was prepared as follows. Appropriate doses of TEOS were added to 15 mL of 1-PrOH, and then 50 μL of 0.1 M hydrochloric acid was added to the solution. After stirring for 1 h at room temperature, $M(OR)_n$ were added to the stirred solution in an atomic ratio of M/Si = 5/95, and the mixtures were further stirred at 70 °C for 30 min. The solution was diluted with 1-PrOH, and the final concentration of the total metal atoms (M + Si) in the precursor solution was adjusted in 40 mM for the films of <100-nm thickness and 80 mM or 100 mM for the films of ≥100-nm thickness.

The precursor sols were spin-coated onto the ITO substrate at 3000 rpm for 40 s by a Mikasa 1H-D7 spin coater. The deposited gel layer was hydrolyzed by blowing hot air for 30 s (Iuchi hot gun), and the substrate was cooled to room temperature by blowing cold air for 20 s. These cycles of spin-coating, hydrolysis and cooling were repeated 6−40 times and the gel films thus obtained were annealed at 400 °C for 15 min. The thickness of films was adjusted by changing the cycle number. The combination of deposition and annealing was repeated more than 3 times, and the final annealing was performed at 450 °C for 1 h. ITO-coated glass slide (ITO layer: 40-nm thick) was used as an electrode substrate. ITO substrate was purchased from Aldrich and the surface was cleaned by sonicating in ethanol for 3 min before film deposition.

The thicknesses of a-$M_{0.1}Si_{0.9}O_x$ films were measured by scanning electron microscopy (SEM) (JEOL JSM-6500F). The specimens for SEM observations were coated with Pt. The surface roughness of films was characterized by atomic force microscopy (AFM) (SII SPA-400). The cross-sectional high-resolution transmission electron microscopy (HRTEM) was performed by JEOL JEM-2100F/SP at an acceleration voltage of 200 kV. Some of ultrathin specimens for the cross-sectional HRTEM observation were prepared from the film sample formed on Si wafer (100) by using a focused ion milling (Gatan 691). Other TEM specimens were prepared from film samples formed on electropolished Al plates (99.99%, 10 mm × 10 mm × 0.5 mm) by using an ultramicrotome (Leica Ultracut-S). X-ray photoelectron spectroscopy (XPS) was carried out with JEOL JPC-9010MC to measure the M/Si atomic ratio of the film. The depth profile of films was also characterized by Rutherford backscattering spectrometry (RBS). The specimens for RBS measurement were prepared on an electropolished Al plate. Temperature desorption spectroscopy (TDS) was performed for 10 × 10 mm^2-size specimens using an ultrahigh vacuum chamber system (ESCO TDS1400) equipped with a quadruple mass analyzer and infrared lamp heater. The spectra were recorded during heating from 50 to 700 at 30 °C min^{-1} under the initial pressure of 2.0 × 10^{-7} Torr. For the measurement, the specimens were deposited on a Si wafer and pretreated by annealing at 400 °C for 12 h in dry air.

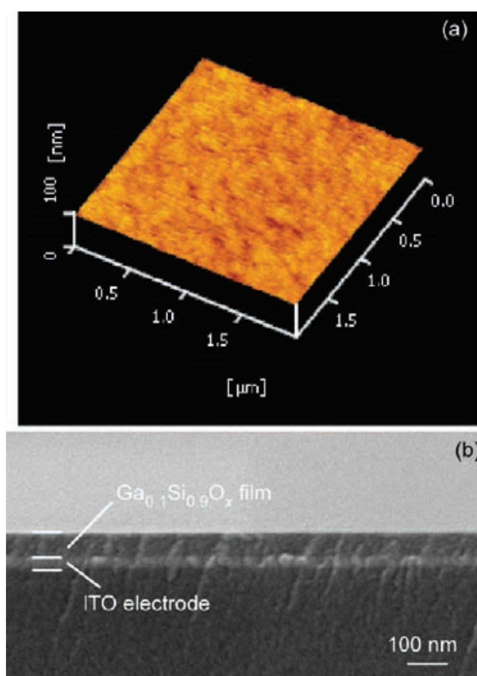

Figure 1. (a) AFM image and (b) cross-sectional SEM image of 100-nm thick $Ga_{0.1}Si_{0.9}O_x$ film.

Proton conductivities along thickness direction of a-$M_{0.1}Si_{0.9}O_x$ films were measured by the ac impedance method. Pt electrodes (100-nm thickness, 1 mm Φ) were deposited on the top of the silicate films by ion etcher (JEOL JFC-1100) through a shadow mask to form a Pt/a-$M_{0.1}$-$Si_{0.9}O_x$/ITO stack. The electrical lead of Au fine wire (0.05 mm Φ) was attached to the top and bottom electrodes by using Au paste (Nilaco). The impedance spectroscopy measurement was carried out for the stack by the frequency response analyzer (Solartron 1260) in a frequency range of 10−10^7 Hz at ac amplitude of 20 mV. The specimens were first heated to 400 °C and kept at this temperature for 12 h under the controlled atmosphere, and then cooled to given temperatures of impedance measurement. All the measurements were carried out under dry and wet atmospheres after an hour of thermal equilibration at each temperature. The proton conductivity, σ, of a film was measured in nonhumidified, 'dry' air which was prepared by flowing a mixed gas of ultrapure O_2 and Ar (99.999%) at a molar ratio of O_2/Ar = 1/4 through a water remover column at a rate of 100 cm^3 min^{-1}. The conductivity of some specimens was also measured in H_2O/air atmosphere (p_{H2O} = 0.042 kPa) and in the D_2O/air atmosphere (p_{D2O} = 0.042 kPa), denoted by σ^{H2O} and σ^{D2O}, respectively, in order to check the H/D isotope effect of σ.

RESULTS

Preparation. The $M_{0.1}Si_{0.9}O_x$ thin films prepared here were an amorphous phase, as shown in the previous reports.[26] All the films uniformly grew over a wide area in thickness precision of nm without pinholes, cracks, or aggregates of particles (Figure 1). The film surface was very smooth in agreement with typical features of glassy film (Figure 1a). Typically, the root-mean-square roughness of the surface is within ±0.8 nm. The thickness increment of these films in a single coating cycle turned out to be

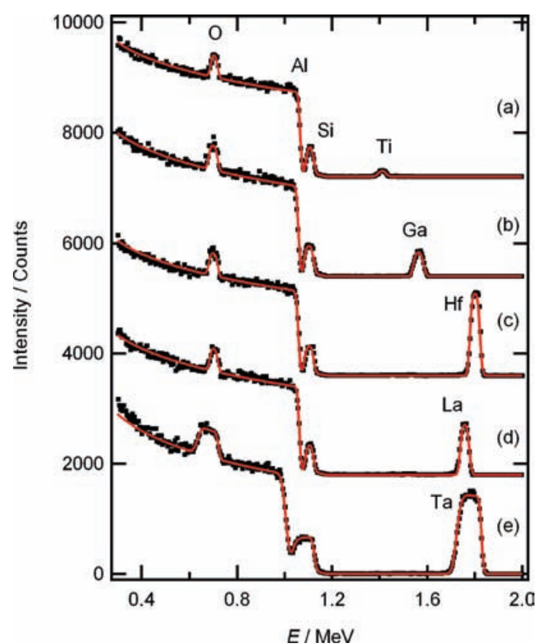

Figure 2. RBS spectra of a-$M_{0.1}Si_{0.9}O_x$ films. M = (a) Ti, (b) Ga, (c) Hf, (d) La, and (e) Ta. Dotted line is the measured data, and solid line, the simulation. The thickness of Ti, Ga, Hf, and La specimens is about 100 nm, and that of Ta is about 200 nm.

Table 1. Chemical Composition of Amorphous Silicate Thin Films Determined by RBS

M	thickness/nm	composition	density/10^{23} atoms cm^{-3}
Ti	100	$Ti_{0.085}Si_{0.915}O_{2.04}H_{0.08}$	0.60
Ga	120	$Ga_{0.126}Si_{0.874}O_{2.02}H_{0.2}$	0.74
La	100	$La_{0.091}Si_{0.909}O_{2.08}H_{0.25}$	0.56
Hf	100	$Hf_{0.095}Si_{0.905}O_{2.05}H_{0.1}$	0.61
Ta	180	$Ta_{0.089}Si_{0.911}O_{2.12}H_{0.15}$	0.69

about 2−5 nm for 40 mM solution. The mole fraction of M atoms, M/(M+Si), in films was 0.1 ± 0.04 in every composition at all the thickness ranges, as checked by XPS measurement. The fraction was invariably greater than those of the corresponding precursor sol (0.05), since the unreacted fraction of TEOS (bp ≈ 170 °C) may be removed from the ultrathin deposited layer by evaporation during the hot-air-blow process after spin coating.

RBS of a-$M_{0.1}Si_{0.9}O_x$ films (M = Ti, Ga, Hf, La, and Ta) with thickness of about 100 nm prepared on the Al plate was measured in order to determine the precise composition (Figure 2). RBS of the as-prepared films is composed of clear peaks of M, Si, and O and the broad background due to the Al substrate, and carbon impurities were not detected. The composition gradients along the thickness were not observed in every case. The simulation was performed with the fixed value of thickness determined by electron microscopy. The simulation of RBS indicates the chemical composition of the film as indicated in Table 1, when the charge neutrality was compensated by protons. The best fitting was obtained with the density of 0.56−0.70 × 10^{23} atoms cm^{-3} for as-prepared samples with any thickness. This density is consistent with the density of pure silica glass, 0.65 × 10^{23} atoms cm^{-3},[28] indicating that the silicate films prepared by our sol−gel process are made of the densely packed oxide-glass layer. The mole fraction of M atoms is about 0.1 in every composition.

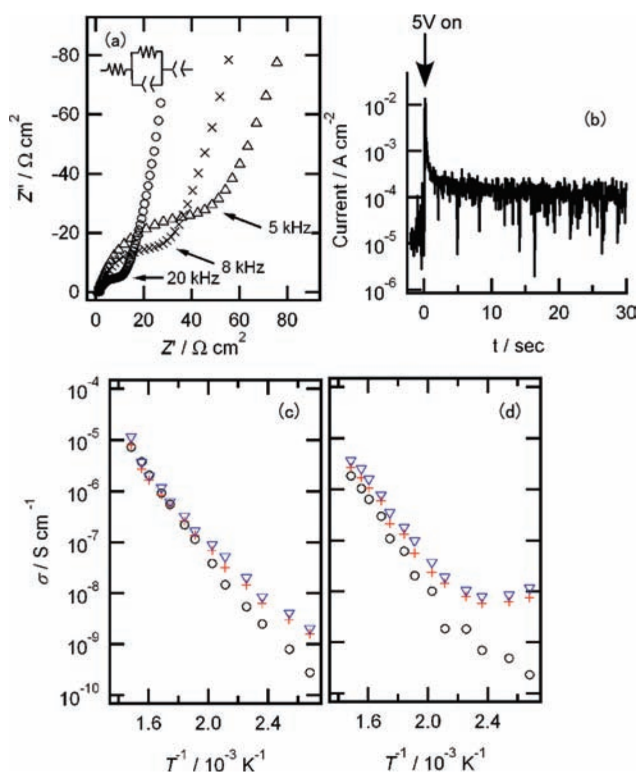

Figure 3. (a) Cole−Cole plots of impedance spectra of 150-nm thick $Ga_{0.1}Si_{0.9}O_x$ films at 350 °C (○), 320 °C (+), and 300 °C (Δ). (b) Current decay curve of the film at 400 °C in dry air by applying dc voltage of +5 V. Arrhenius plots of proton conductivity of 150-nm thick films of (c) $Ga_{0.1}Si_{0.9}O_x$ and (d) $Ti_{0.1}Si_{0.9}O_x$. The conductivities in dry air (○, black), in H_2O/air (▽, blue) and in D_2O/air (+, red).

All films apparently contain the hydrogen impurity with the molar ratio of M/H = 1/1−1/2 due to the existence of excess oxygen atoms.

Proton Conductivity. All of the a-$M_{0.1}Si_{0.9}O_x$ films exhibit impedance spectra characteristic of ion-conducting film, that is, a small semicircle in the high-frequency region and a spike in the low-frequency region in Cole−Cole plots.[29] A typical example of the impedance spectra of 150-nm thick a-$Ga_{0.1}Si_{0.9}O_x$ film is shown in Figure 3a. The high-frequency semicircle can be attributed to the impedance response of ionic conduction of the film along the thickness direction. It becomes smaller as temperature is raised. Additional semicircles that may be related to the conduction through grain boundary or impurity layer do not appear at any temperature. The low-frequency spike corresponds to the charge buildup at the interface of film/electrode,[29] indicating that the charge transfer occurs across the film and the electron-conductive electrode is negligibly small. Figure 3b shows the time transient curve of the dc current of the film. The current abruptly decreases when the dc bias is applied, and the decay is terminated within a few seconds. The terminal current is 2 orders of magnitude smaller than the initial peak current, suggesting that an electronic contribution to overall conductivity in silicate film is negligibly small. Hence, proton conductivity (σ) of a-$M_{0.1}Si_{0.9}O_x$ films can be determined from the contribution of the high-frequency semicircle by an equivalent circuit analysis with the model shown in Figure 3a.[26,29]

Plots c and d of Figure 3 show the proton conductivities of 150-nm thick a-$Ga_{0.1}Si_{0.9}O_x$ film and 140-nm thick a-$Ti_{0.1}Si_{0.9}O_x$ film, measured in dry, hydrated and deuterated air. σ^{H2O} of

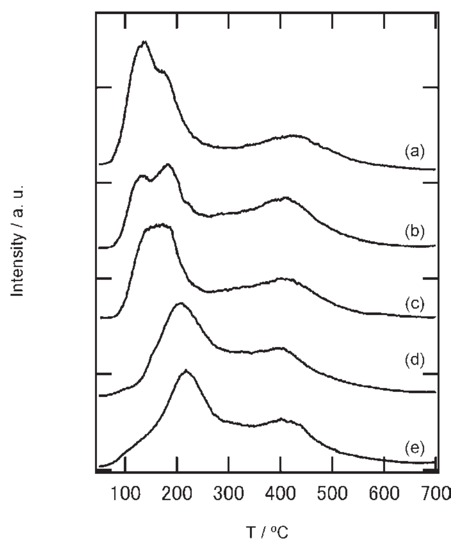

Figure 4. TDS of water ($m/z = 18$) of a-$M_{0.1}Si_{0.9}O_x$ films with M = (a) Ga, (b) Ta, (c) Hf, (d) La, and (e) Ti.

a-$Ga_{0.1}Si_{0.9}O_x$ film is almost the same as σ in dry air at T > 220 °C, but the former is larger than the latter at T < 220 °C because the activation energy E_a of σ^{H2O} changes at around 250 °C from 0.7 to 0.9 eV. The humidity dependency of a-$Ga_{0.1}Si_{0.9}O_x$ film is analogous to that of a-$Al_{0.1}Si_{0.9}O_x$ films.[18] The increment of a conductivity by moisture is more pronounced in $Ti_{0.1}Si_{0.9}O_x$. σ^{H2O} of $Ti_{0.1}Si_{0.9}O_x$ is larger than that of σ in dry air by a factor of about 2 at T > 200 °C, but the E_a of σ^{H2O} is similar to that in dry air at the same temperatures. In addition, the σ^{H2O} becomes almost constant, and σ^{H2O} is larger than that of σ in dry air by a factor of more than 10 at T < 200 °C. The enhancement of the conductivity at relatively low temperatures by moisture is due to the additional protonic carriers on Lewis acid sites, which are given by the water adsorption onto an oxygen vacancy site.[27,30] Both films show the clear H/D effect[31] on proton conductivity in the measured temperature ranges, and σ^{D2O} is lower than σ^{H2O} by a factor of 1.1−1.4 even though the temperature dependency of σ^{D2O} is very similar to that of σ^{H2O} in every thickness. Other $M_{0.1}Si_{0.9}O_x$ films also show the similar isotope effect in conductivity. Thus, it is confirmed that the proton conduction is dominant in a-$M_{0.1}Si_{0.9}O_x$ films at temperatures below 400 °C.

Thermal desorption spectroscopy (TDS) was performed for a-$M_{0.1}Si_{0.9}O_x$ films (M = Al, Ga, Ta, Hf, La, and Ti) with about 100-nm thickness (Figure 4). The amount of desorbed CH_4 ($m/z = 16$), CO ($m/z = 28$), and CO_2 ($m/z = 44$) was very small in the measured temperature range, suggesting that the desorbed waters are not a product by combustion of contaminant organic species. There is an intensive desorption of water gas in all films at a relatively low temperature below 250 °C owing to desorption of the adsorbed water.[27,30] Such water is not concerned with the proton conductivity discussed later since the measurements were performed by cooling a sample from 400 °C to given temperatures of measurement with nonhumidified atmosphere. The films show a single desorption peak at temperatures above 400 °C, which is assigned to the decomposition of the Brønsted acid site.[30] It is obvious that this type of proton can be retained under the conductivity measurement conditions.

The proton conductivities of a-$M_{0.1}Si_{0.9}O_x$ films with various thicknesses were measured in dry air (Figure 5). Apparently, the relatively high proton conductivity at elevated temperatures ($T \geq 200$ °C) is a linear Arrhenius relationship, although some films show the upward deviation from the linear relationship at temperatures below 200 °C by the effect of adsorption of residual water. Accordingly, it is concluded that the conductivity of the silicate films at temperatures above 200 °C in dry air is related solely to the proton on the Brønsted acid site, if any, at all the thicknesses and compositions. Hereafter, the thickness dependency of σ at $T \geq 200$ °C in dry air is mainly discussed.

In M = Ti and Hf, σ is not varied by thickness in the measured temperature range, and σ of the thinnest films (about 30 nm) is comparable to those of the thickest films (>400 nm) at any temperature. The E_a of conductivity above 220 °C is 0.9 and 0.8 eV for Ti and Hf specimens, respectively. σ at 250 °C is plotted as a function of d in Figure 6, indicating that σ of these films is almost constant in the measured thickness range.

σ of the Ga and Ta films is apparently changed by thickness in the measured temperature range. σ of an a-$Ga_{0.1}Si_{0.9}O_x$ film is not dependent on the thickness in d > 300 nm, and it linearly increases with temperature with E_a of 0.9 eV above 220 °C. When d is <300 nm, the value of σ apparently increases with decreasing thickness, and the increment of σ is almost saturated at a thickness of <50 nm. Furthermore, an Arrhenius plot of σ of the films with d < 180 nm turns to be linear with E_a of 0.8 eV in the measured temperature range even though that of the films with d > 200 nm reveals the change of E_a at round 200 °C. σ at 250 °C is clearly elevated in a power law by reducing d from 300 to 60 nm and the increment is saturated in d < 50 nm (Figure 6). A scaling index, τ, of a-$Ga_{0.1}Si_{0.9}O_x$, which is determined by the slope of the plots in Figure 6 in the region of 300 nm < d < 60 nm, is slightly larger than that of a-$Al_{0.1}Si_{0.9}O_x$ ($\tau = 2.3$),[18] as listed in Table 2. Hence, the σ at 250 °C of 50-nm thick film turns out to be larger than that of 300-nm thick film by 50 times. a-$Ta_{0.1}Si_{0.9}O_x$ films also reveal the increase of σ by decreasing thickness in the range from 220 to 110 nm, and the rate of increase is lowered in films with d < 100 nm; thus, σ gradually increases by decreasing the thickness in the range from 80 to 50 nm (Figures 5 and 6). E_a is about 0.7 eV in films with d < 200 nm and 0.8 eV in films with d > 250 nm, as determined from the slope of the Arrhenius plots above 200 °C. Therefore, a-$Ta_{0.1}Si_{0.9}O_x$ film reveals size-scaling of σ at 250 °C in the d range from 250 to 80 nm with τ of 2.7, and σ at 250 °C of 50-nm thick film is 30 times larger than that of 250-nm thick film.

σ of a La film is slightly increased by reducing the thickness in films with d < 80 nm, but the increment is not remarkable compared to the films with M = Ta and Ga (Figures 5 and 6). The E_a of conductivity above 220 °C is 1.0 eV at any thicknesses.

Numerical Analysis. The finite-size scaling of conductivity is characteristic of the percolative conduction system below critical threshold P_c.[32−35] Therefore, it is presumed that Ga and Ta films have an ion-conducting pathway distributed randomly through the poorly conducting matrix as is the case with a-$Al_{0.1}Si_{0.9}O_x$.[18] Figure 7a is the two-dimensional (2-D) representation for the finite-size scaling of the conductivity of a silicate thin film.[18] Here, the glass network of silicate is approximated by a square lattice with a lattice constant, λ, and the black bond represents the highly conductive ionic pathway with a unit length of λ. A black bond randomly occupies a lattice edge with a constant probability P of 0.35 below a percolation threshold P_c of 2-D bond percolation (0.5).[32] In such subcritical systems, the clusters (groups of neighboring bonds of various average lengths $[l]$)

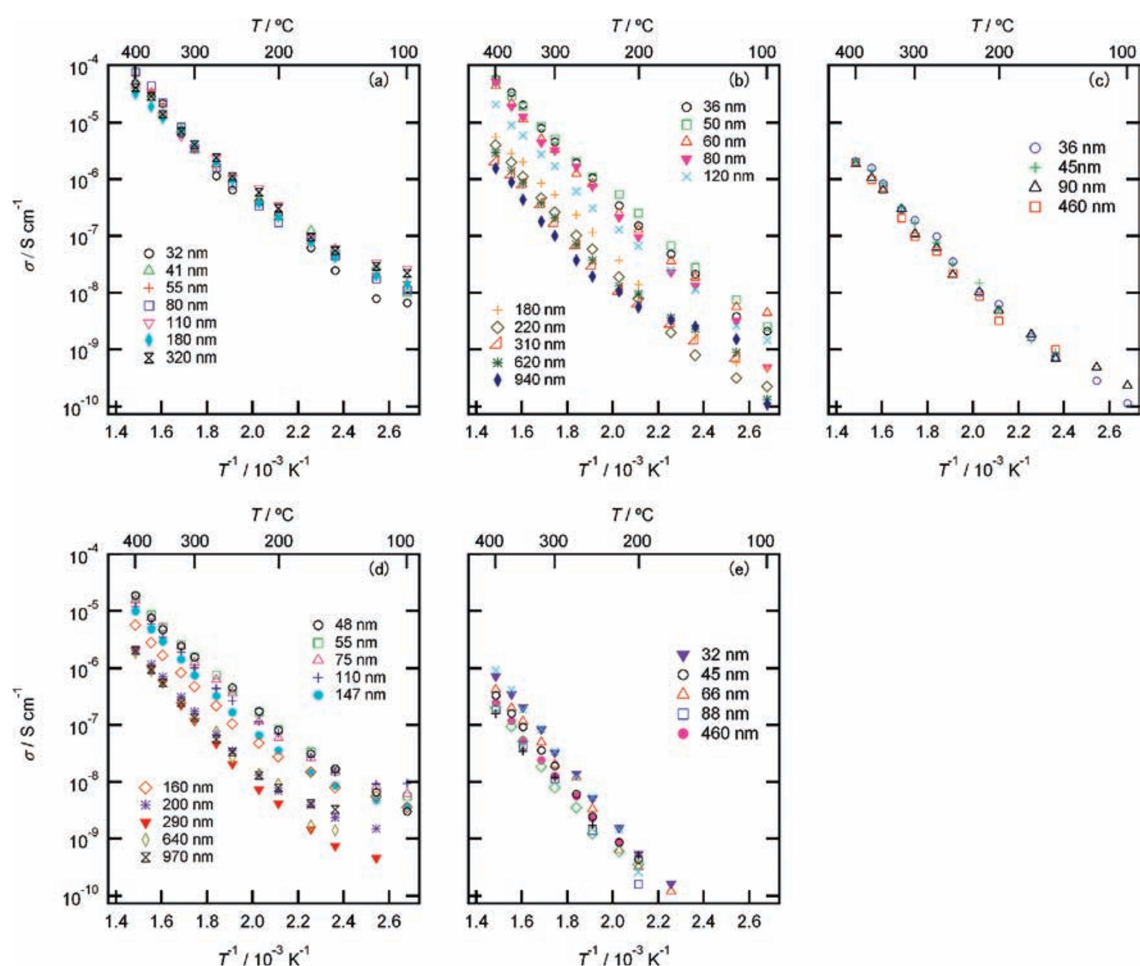

Figure 5. Arrhenius plots of σ of amorphous $M_{0.1}Si_{0.9}O_x$ films with different thicknesses, measured in dry air. M = (a) Hf, (b) Ga, (c) Ti, (d) Ta, and (e) La.

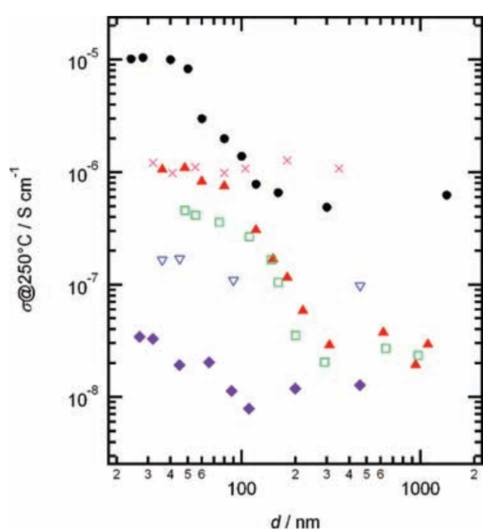

Figure 6. Log−log plot of σ at 250 °C in dry air vs d for a-$M_{0.1}Si_{0.9}O_x$ films. Al (● black), Hf (× pink), Ga (▲ red), Ti (▽ blue), La (♦ purple), and Ta (□ green). The measured data of Al is the same as that reported elesewhere.[18]

accumulate inside the glass, and the number of clusters of a finite length l (N) increases with decreasing l by following.[32]

$$N(l, \zeta) \propto (l/\zeta)^{-\tau} \qquad (1)$$

Table 2. Size-Scaling Properties of Proton Conductivity at 250°C of $M_{0.1}Si_{0.9}O_x$ Films[a]s

M	τ	ζ/nm	R_1/Ω	R_2/Ω	F_2/%	λ/nm
Al	2.3	120	6.3×10^{10}	2.2×10^{8}	9.2	40
Ga	2.8	300	1.5×10^{13}	2.1×10^{10}	15	65
Ta	2.7	220	4.9×10^{12}	1.0×10^{10}	3.8	100

[a] Scaling index τ and coherent length ζ were determined by measured data shown in Figure 5, and other properties were determined by numerical analysis.

This is so-called 'finite-size scaling' of the clusters. Here, ζ is a correlation length (i.e., average length of the largest cluster in the system). In $d > \zeta$, the conductive clusters become insulated in a poorly conducting matrix, and a film remains in the low (normal) conductive phase. The conductive pathway penetrating between both electrodes is formed at $d \approx \zeta$, and the conductivity increases in $\zeta < d < \lambda$ since more conductive clusters connect between both with decreasing d by following eq 1. When d is close to λ, the increase of σ is terminated. The features of thickness-dependent conductivity of a-$M_{0.1}Si_{0.9}O_x$ films are coincident with those phenomena of a percolation system.

To establish this idea, a 3-D random resistor network[36] serving as a model for percolative ionic conduction of a-$M_{0.1}Si_{0.9}O_x$ films (M = Al, Ga, and Ta) is considered (Figure 7b). It consists of two

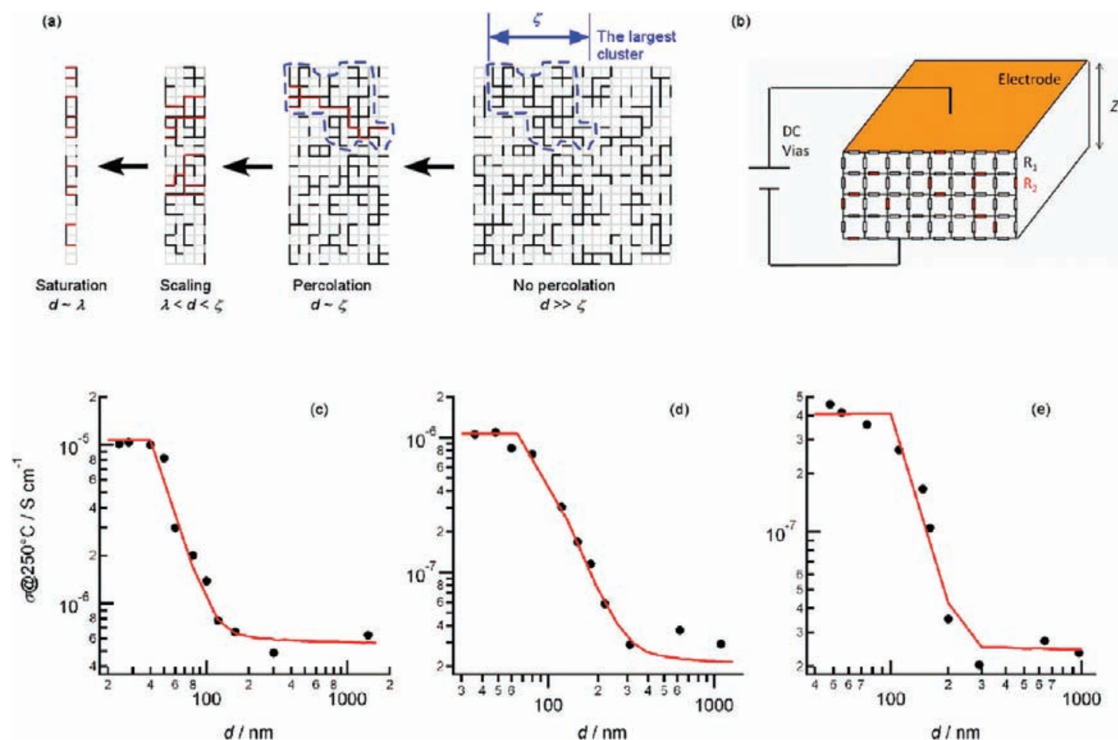

Figure 7. (a) Two-dimensional bond percolation in 20 × 20 square lattice. The calculation is performed with a bond population of 0.35. (b) Three-dimensional (3-D) cubic-type random resistor network used for the numerical calculation. The numerical simulation best fit to the thickness-dependent conductivity of (c) $Al_{0.1}Si_{0.9}O_x$, (d) $Ga_{0.1}Si_{0.9}O_x$, and (e) $Ta_{0.1}Si_{0.9}O_x$ with the percolation model depicted in (b). In (c), (d), and (e), black circles represent the experimental data, and red lines, the simulation.

kinds of Ohmic resistors, R_1 and R_2 with $R_1 > R_2$. R_1 represents the poorly conducting glass matrix, while R_2 represents the randomly distributed proton-conducting pathways. R_1 and R_2 occupy a lattice edge of the simple cubic-type cell, so that the unit length of the resistors is represented by the lattice constant λ. F_2 is fraction of R_2 and is below the threshold of 3-D bond percolation of 24.9%.[32] In order to simulate the thickness-dependent conductivity of a-$M_{0.1}Si_{0.9}O_x$, the conductivities of resistor networks with a size of 200 × 200 × z resistors were numerically calculated by varying the normalized thickness z with parameters of R_1, R_2, F_2, and λ. The top and bottom faces of the resistor lattice are attached to electrodes, and a constant voltage is applied between both electrodes. In the stationary condition, the first Kirchhoff's law must be obeyed for the current flow at each node, and thus the effective conductivity of the resistor network between electrodes can be calculated from the overall current flow given by sum of current flows at every node. A result by numerical simulation is presented in Figure 7. An optimal fitting can be achieved for Al, Ga, and Ta films with the parameters listed in Table 2. The thickness-dependent σ of $Al_{0.1}Si_{0.9}O_x$ and $Ga_{0.1}Si_{0.9}O_x$ films is replicated well by the percolative network model, but that of $Ta_{0.1}Si_{0.9}O_x$ films is slightly deviated from the simulated. The details are discussed later. In every case, R_2 is lower than R_1 by 2 or 3 orders of magnitude, and the fraction of R_2, F_2, is much smaller than P_c. The dimensions of the conducting path unit inside glass films are several 10's of nanometers. These results clearly demonstrate that the thickness-dependent conductivity of a-$M_{0.1}Si_{0.9}O_x$ is identical to finite-size scaling of the cluster of the proton-conducting pathway in the range of a few 10's to 100's of nanometers.

Microstructure. The microstructure of amorphous $M_{0.1}Si_{0.9}O_x$ films (M = Al, Ta, Ga, and Hf) was investigated by HRTEM (Figure 8). Every film has apparent microstructural features made of the dark micro domains and the surrounding bright matrix, both of which are an amorphous phase. The near-spherical domains with widths <10 nm are interconnected to each other so as to form the wormlike domains having an average length of several 10's of nanometers. Such a domain structure is observed whenever the specimens are prepared by ion-milling or microtome, indicating that the irradiation of the ion beam does not affect the microstructural evolution. The contrast between dark domain and bright matrix shows that the concentration of heavier atoms in the dark domain is higher than that in the bright matrix. The difference in composition between the dark domain and the bright matrix moiety is not remarkable since point analysis by STEM-EDX with beam size <4 nm for $Ga_{0.1}Si_{0.9}O_x$ film typically shows that the mole fraction of Ga atoms in the dark domain is 0.12 ± 0.06 and that in bright matrix is in the range of deviation (0.09 ± 0.04). Furtheremore, the microstructural contrast in HRTEM of Al film cannot be attributed to the minor fluctuation in composition because the atomic scattering factor of Al is close to that of Si. Several authors reported the fluctuations in both density and composition of a silica-based glass system taking place on nanometer-length scale.[37−43] Especially the multicomponent silicate glasses SiO_2−MO_n prepared by sol−gel technique are reported to involve heterogeneous microstructures consisting of the condensed M-rich microphase and the uncondensed M-poor microphase due to the spinodal-type decomposition.[40−43] TEMs of such SiO_2−Al_2O_3 glass have shown the clear contrast between the dark and bright moieties corresponding to Al-rich and Al-poor microphases, respectively,

because Al-rich domain tended to be the high-density microphase owing to the difference in iconicity of Al—O and Si—O bonds.[41] These features are in agreement with the microstructural properties of our $M_{0.1}Si_{0.9}O_x$ thin films. Accordingly, the microstructural contrast in the HRTEM of $M_{0.1}Si_{0.9}O_x$ suggests that both the density and the concentration of M in dark domains are higher than those in bright matrices. Hereafter, the dark domain and bright matrix as observed by TEM are represented as a condensed domain and uncondensed matrix, respectively.

DISCUSSIONS

The proton conductivity of a-$M_{0.1}Si_{0.9}O_x$ films dramatically increases by reducing thickness to <100 nm in the cases of M = Ga, Al, and Ta, although the Hf, Ti, and La films do not reveal this remarkable enhancement when the thickness is decreased. This finite-size effect of σ in Al, Ga, and Ta films is based on size scaling of the network built up by the interconnecting conduction pathways in the nanometer range. Such a pathway randomly distributes in the relatively low-conducting glass matrix, and its volume fraction F_2 appears to be much smaller than percolation thresholds P_c (0.25 for bond percolation in 3-D) in every composition (Table 2).

In all cases of Al, Ga, and Ta, the λ that is an average length of the building block of the percolative protonic pathways is in the range of several 10's of nanometers (Table 2). Vergri et al. estimated by the Monte Carlo simulation that Li—B—O glass exhibits the size scaling of Li ion conductivity since Li ions can more easily jump between the sites on nonbridged oxygen (NBO) of borate than between other sites so that the clustering of NBO sites poses Li ion channel penetrating through the glass network.[17] The λ in this model is close to the ionic jump distance between the adjacent NBO sites and is less than ten nanometers. Consequently, the Li ion conductivity across the a-Li—B—O thin film may continuously increase until the thickness decreases down to <10 nm. Recently, this phenomemon of ion conducting a-Li—B-O thin films was experimentally substantiated by Berkemeier et al.[15,16] Such a model on the basis of the site-to-site defect motion does not match to our case. The λ of a silicate film is clearly larger than the ionic jump distance by 1 or 2 orders of magnitude.

It is clear that the average length of the condensed wormlike domain in a-$M_{0.1}Si_{0.9}O_x$ is corresponding to the λ determined by the numerical simulation. In TEM photograph, the condensed domain is seen to form the network structure penetrating through the uncondensed matrix at any composition (Figure 8). Furthermore, the volume fractions of the condensed domains in Al, Ga and Ta films are smaller than those of the uncondensed matrix and are estimated to be in range of 7—23% by using the area fractions of the dark domains in TEM image (30—40%). These values are clearly smaller than P_c of 3-D bond percolation (25%), although they are slightly larger than F_2 determined by numerical analysis (Table 2). The volume fraction of the condensed domains in Hf film that do not reveal conductivity scaling is clearly larger than those of the Al, Ga, and Ta films and is estimated to be more than 35%. This value is larger than P_c of 3-D bond percolation. This result can be explicable if the condensed domain serves as an ion-conducting pathway, since the film which involves the large population over the threshold must reveal the thickness-independent, relatively high conductivity. On the basis of these results, the condensed domains

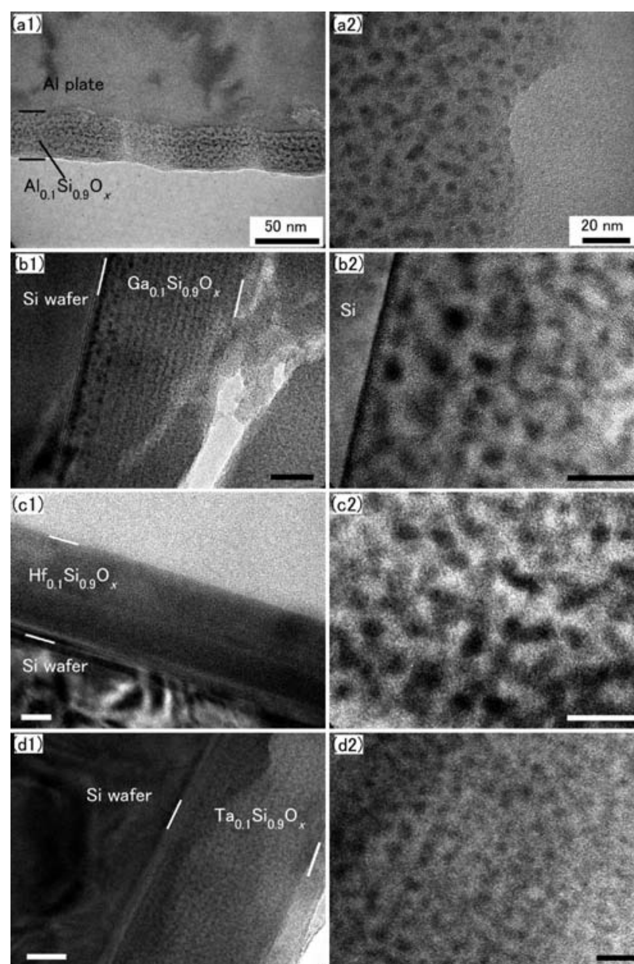

Figure 8. Cross-sectional HRTEM images of $M_{0.1}Si_{0.9}O_x$ films. (a1) and (a2) Al, (b1) and (b2) Ga, (c1) and (c2) Hf, and (d1) and (d2) Ta. The images (a2), (b2), (c2), and (d2) are the magnification of (a1), (b1), (c1), and (d1), respectively. Scale bar in (a1), (b1), (c1), and (d1) is 50 nm, and scale bar in (a2), (b2), (c2), and (d2) is 20 nm.

can be identified as the ion-conducting pathway in the a-$M_{0.1}Si_{0.9}O_x$ film.

As shown in Figure 7, the thickness dependency of σ of Ta films is not perfectly replicated by the simulation with a simple cubic-type cell. The scaling index apparently changes at ~100 nm, and the increment of σ is still unsaturated at ~50 nm thickness (Figure 6). These indicate that the λ of Ta films is widely distributed in the sub-100-nm length region. Other investigations are needed to clarify more detailed mechanism.

Previously, we reported that the most feasible transport process in a-$M_{0.1}Si_{0.9}O_x$ is the thermally activated jump of protons between the adjacent Brønsted acid sites on the —Si(M)—O— network.[18] The redistribution of the acid site population caused by the fluctuation of the glass network may change the potential distribution for ionic diffusion and/or the carrier density in the film. Hence, the condensed domains are speculated to possess a lower barrier height for proton hopping and a higher carrier density than the uncondensed matrix. This is in agreement with the result that E_a of the Al, Ga, and Ta films of $d < \zeta$ is smaller than those of the thicker films (Figure 5). The Brønsted acid center of a-$Al_{0.1}Si_{0.9}O_x$ is given by the formula of $[AlO_4H(SiO)_4]$,[18] indicating that the Al/Si molar ratio of the

film (1/9) is smaller than that of the ideal acid network (1/4) which is built up by the repeat of the acid centers. Therefore, the relatively high concentration of the M atom in the condensed domains is consistent with its lowered resistance.

It was reported that the mesoscopic fluctuation of glass is due to freezing in the divergence of viscous liquid near liquid−glass transition.[37,38] The hydrolysis of TEOS is much slower than that of other metal alkoxides.[44] Therefore, it is speculated that the different kinetics of hydrolysis between TEOS and other metal alkoxides during sol−gel transition may encourage the formation of heterogeneous microstructures of the resultant oxide films in the case of a sol−gel derived glassy film. The reactive metal alkoxides transition to the inorganic oxide layer without heating by moisture-catalyzed hydrolytic condensation. Some of the TEOS will be incorporated into the deposited gel layer without hydrolysis due to the relatively low sensitivity to water, and it changes to the oxide moiety by subsequent heating. In the latter case, a highly condensed network of −Si−O−Si(M)−O− is not developed because of extensive deformation of the network during removal of a large amount of the organic residues. Therefore, it appears that the oxide moieties formed directly by the hydrolytic condensation tend to become the condensed domain, and the moieties developed from the unhydrolyzed TEOS turn to the uncondensed matrix as a result. The phase separation due to the immiscibility and the local crystallization is not intensive in our case because of the relatively low process temperatures ∼450 °C. Understanding the relationship between the microstructure evolution and the preparation conditions such as temperature, humidity, viscosity of precursor, dopant effect, and so on is of great importance in order to efficiently tune the ionic conductivity of the glassy films.

CONCLUSIONS

It was demonstrated that finite-size scaling of proton conductivity of amorphous $M_{0.1}Si_{0.9}O_x$ thin films (M = Al, Ga, and Ta) is based on the heterogeneous microstructures involved by the nanoscale fluctuation in density and composition. The films are made of the wormlike condensed domain of several 10's of nanometers in length and the surrounding uncondensed matrix. The conductance of the former is higher than that of the latter by at least 2 orders of magnitude, and thus, the condensed domain penetrating through the uncondensed matrix performs the role of proton-conducting pathway. The volume fractions of condensed domain in these films (<0.2) are smaller than the threshold for 3-D bond percolation. Therefore, the conductive networks of interconnected domains with a finite length are insulated inside the film when the film thickness is very large. When the thickness is in range of the average length of the networks, the protonic pathway connecting both electrodes is formed, and the conductivity across the film increases. Consequently, σ of a film with M = Al, Ta, and Ga increases in a power law by decreasing thickness into less than 100 nm, and σ of several 10's of nanometers in thickness is higher than that of a few 100 nm by more than 1 order of magnitude. The preceding results affirm that the topological properties of the microstructures ranging from the domain shape to the connectivity of the domain network are critical to the protonic conductivity of the sol−gel-derived silicate films. Moreover, the mesoscopic fluctuation is characteristic of the 'nonequilibrium', disordered system including inorganic glass, polymers, inorganic/organic hybrids, and so on,[45] so that these topological considerations are extremely useful for a wide variety of glassy ion-conducting systems. The present results reveal the new way for the tailor-made development of fast-ion conductors.

AUTHOR INFORMATION

Corresponding Author
y-aoki@eng.hokudai.ac.jp

ACKNOWLEDGMENT

We are grateful to Dr. G. Schmitz and Dr. F. Berkemeier of Universität Münster for providing a source code for numerical simulation. This work was financially supported by the Grant-in-Aid of JSPS for Scientific Research on Young Scientists (A) and by the Global COE Program (Project No. B01: Catalysis as the Basis for Innovation in Materials Science) from the Ministry of Education, Culture, Sports, Science and Technology, Japan.

REFERENCES

(1) Steele, B. C. H.; Heinzel, A. *Nature* **2001**, *414*, 345.
(2) Jacobson, A. J. *Chem. Mater.* **2010**, *22*, 660.
(3) Armand, M.; Tarascon, J.-M. *Nature* **2008**, *451*, 652.
(4) Birke, P.; Chu, W. F.; Weppner, W. *Solid State Ionics* **1997**, *93*, 1.
(5) Badwal, S. P. S.; Ciacchi, F. T. *Adv. Mater.* **2001**, *13*, 993.
(6) Strukov, D. B.; Snider, G. S.; Stewart, D. R.; Williams, R. S. *Nature* **2008**, *453*, 80.
(7) (a) Waser, R.; Dittmann, R.; Staikov, G.; Szot, K. *Adv. Mater.* **2009**, *21*, 2632. (b) Waser, R.; Aono, M. *Nat. Mater.* **2007**, *6*, 833.
(8) (a) Maier, J. *Nat. Mater.* **2005**, *4*, 805. (b) Maier, J. *Prog. Solid State Chem.* **1995**, *23*, 171. (c) Maier, J. *Solid State Ionics* **2002**, *154*−*155*, 291. (d) Sata, N.; Eberman, K.; Maier, J. *Nature* **2000**, *408*, 976.
(9) Matsumoto, H.; Furuya, Y.; Okada, S.; Tanji, T.; Ishihara, T. *Electrochem. Solid State Lett.* **2007**, *10*, P11–P13.
(10) Garcia-Baririocanal, J.; Rivera-Calzada, A.; Verela, M.; Sefrioui, Z.; Iborra, E.; Leon, C.; Pennycook, S. J.; Santamaria, J. *Science* **2008**, *321*, 676.
(11) Tuller, H. L. *Solid State Ionics* **2000**, *131*, 143–157.
(12) Park, J. S.; Kim, Y. B.; Shim., J. H.; Kang, S.; Gür., T. M.; Prinz, F. B. *Chem. Mater.* **2010**, *22*, 5366.
(13) Schoonman, J. *Solid State Ionics* **2003**, *157*, 319.
(14) Gil, Y.; Umurhan, O. M.; Riess, I. *Solid State Ionics* **2007**, *178*, 1.
(15) Berkemeier, F.; Abouzari, M. R. S.; Schmitz, G. *Phys. Rev. B* **2007**, *76*, 024205.
(16) Berkemeier, F.; Abouzari, M. R. S.; Schmitz, G. *Ionics* **2009**, *15*, 241.
(17) (a) Vegiri, A.; Varsami, C. E. *J. Chem. Phys.* **2004**, *120*, 7689. (b) Varsami, C. E.; Vegiri, A.; Kamitsos, E. I. *Phys. Rev. B* **2002**, *65*, 104203.
(18) Aoki, Y.; Habazaki, H.; Kunitake, T. *J. Am. Chem. Soc.* **2009**, *131*, 14399.
(19) Hunt, A. G. *Phil. Mag. B* **2001**, *81*, 875.
(20) Dyre, J. C.; Maass, P.; Rolling, B.; Sidebottom, D. L. *Rep. Prog. Phys.* **2009**, *72*, 046501.
(21) Hibino, T.; Akimoto, T.; Iwahara, H. *Solid State Ionics* **1993**, *67*, 71–76.
(22) Kwan, S. M.; Yeung, K. L. *Chem. Commun.* **2008**, 3631.
(23) Norby, T. *Solid State Ionics* **1999**, *125*, 1.
(24) (a) Nagao, M.; Takeuchi, A.; Heo, P.; Hibino, T.; Sano, M.; Tomita, A. *Electrochem. Solid-State Lett.* **2006**, *9*, A105. (b) Nagao, M.; Kamiya, T.; Heo, P.; Tomita, A.; Hibino, T.; Sano, M. *J. Electrochem. Soc.* **2006**, *153*, A1604. (c) Tomita, A.; Kajiyama, N.; Kamiya, T.; Nagano, M.; Hibino, T. *J. Electrochem. Soc.* **2007**, *154*, B1265.
(25) (a) Haile, S. M.; Boysen, D. A.; Chisholm, C. R. I.; Merle, R. B. *Nature* **2001**, *410*, 910. (b) Haile, S. M.; Chisholm, C. R. I.; Sasaki, K.; Boysen, D. A.; Uda, T. *Faraday Discuss.* **2007**, *134*, 17.

(26) Aoki, Y.; Muto, E.; Nakao, A.; Kunitake, T. *Adv. Mater.* **2008**, *20*, 4387.
(27) Aoki, Y.; Habazaki, H.; Kunitake, T. *Solid State Ionics* **2010**, *115*, 115.
(28) Kajihara, K.; Hirano, M.; Uramnoto, M.; Morimoto, Y.; Skuja, L.; Hosono, H. *J. Appl. Phys.* **2005**, *98*, 013527.
(29) (a) Irvine, J. T. S.; Sinclair, D. C.; West, A. R. *Adv. Mater.* **1990**, *2*, 132. (b) Guo, X. X.; Matei, I.; Lee, J.-S.; Maier, J. *Appl. Phys. Lett.* **2007**, *91*, 103102.
(30) Bronnimann, C. E.; Chuang, I.-S.; Hawkins, B. L.; Marciel, G. E. *J. Am. Chem. Soc.* **1987**, *109*, 1562.
(31) Norby, T. *Solid State Ionics* **1990**, *40*−*41*, 857.
(32) Stauffer, D.; Aharony, A. *Introduction to Percolation Theory*; Taylor & Francis: Washington, DC, 1991.
(33) Cheianov, V. V.; Fal'ko, V. I.; Altshuler, B. L.; Aleiner, I. L. *Phys. Rev. Lett.* **2007**, *99*, 176801.
(34) (a) Snow, E. S.; Novak, J. P.; Campbell, P. M.; Park, D. *Appl. Phys. Lett.* **2003**, *82*, 2145. (b) Behman, A.; Ural, A. *Phys. Rev. B* **2007**, *76*, 125432.
(35) Pennetta, C.; Trefán, G.; Reggiani, L. *Phys. Rev. Lett.* **2000**, *85*, 5238.
(36) Kirkpatrick, S. *Rev. Mod. Phys.* **1973**, *45*, 574.
(37) (a) Chanmpagnon, B.; Martinez, V.; Martinet, C.; Le Parc, R.; Levelut, C. *Philos. Mag. B* **2007**, *87*, 691. (b) Levelut, C.; Le Parc, R.; Faivre, A.; Bruning, R.; Chanmpagnon, B.; Martinez, V.; Simon, J.-P..; Bley, F.; Hzaman, J.-L. *J. Appl. Crystallogr.* **2007**, *40*, s512. (c) Le Parc, R.; Chanmpagnon, B.; Guenot, Ph.; Dubois, S. *J. Non-Cryst. Solids* **2001**, *293*−*295*, 366.
(38) (a) Watanabe, T.; Saito, K.; Ikushima, A. J. *J. Appl. Phys.* **2003**, *94*, 4824. (b) Watanabe, T.; Saito, K.; Ikushima, A. J. *J. Appl. Phys.* **2004**, *95*, 2432.
(39) Chen, S.-C.; Dejneka, M. J. *Mater. Res. Soc. Symp. Proc.* **2003**, *751*, 49.
(40) Okada, K.; Otsuki, N. *J. Am. Ceram. Soc.* **1986**, *69*, 652.
(41) Takei, T.; Kameshima, Y.; Yasumori, A.; Okada, K.; Kumada, N.; Kinomura, N. *J. Non-Cryst. Solids* **2001**, *282*, 265.
(42) (a) Karthikeyan, A.; Almeida, R. M. *J. Mater. Res.* **2001**, *16*, 1626. (b) Orignac, X.; Vasconselo, H. C.; Almeida, R. M. *J. Non-Cryst. Solids* **1997**, *217*, 155.
(43) Gonzalez-Oliver, C. J. R.; James, P. F.; Rawson, H. *J. Non-Cryst. Solids* **1982**, *48*, 129.
(44) Pope, E. J. A.; Mackenzie, J. D. *J. Non-Cryst. Solids* **1986**, *87*, 185.
(45) Fernández, L. A.; Martín-Mayor, V.; Verrocchio, P. *Phys. Rev. E* **2006**, *73*, 020501.